

Performance of Pitch and Stall Regulated Tidal Stream Turbines

Ben Whitby, *Student Member, IEEE*, and Carlos E. Ugalde-Loo, *Member, IEEE*

Abstract—Controllers for a pitch and a stall regulated horizontal axial flow, variable-speed tidal stream turbine are developed, and a performance comparison is carried out. Below rated flow speed, both turbines are operated in variable-speed mode so that the optimum tip-speed ratio is maintained. One of the turbines has variable pitch blades, which above rated speed are pitched to feather in order to regulate power. The other turbine has fixed pitch blades and uses speed-assisted stall to regulate power. The control system design behind both strategies is examined in MATLAB, with the performance under turbulent flows, loading and energy yield analysis being evaluated in GH Tidal Bladed. Both strategies provide a satisfactory performance, but the out-of-plane loads on the stall regulated turbine were higher over the entire range of operation. In addition, the dynamic characteristics of the stall regulated turbine require a more complex control design. The results suggest that the pitch regulated turbine would be a more attractive solution for turbine developers.

Index Terms—Control, pitch regulation, stall regulation, synchronous generator, tidal power, tidal stream turbine.

I. INTRODUCTION

IT IS estimated that 20.6 TWh/y could practically be extracted from waters around the U.K. using currently foreseeable tidal stream technologies [1]. This estimate takes into account practical constraints that will affect energy extraction such as fishing, shipping, and designated conservation areas. In [2], it was established that as much as 94 TWh/y could be generated assuming that all areas up to a depth of 40 m are developed. Around the U.K., leases for up to 1.6 GW of wave and tidal devices have been awarded by the Crown Estate [3].

The tidal flow rate at any site will vary over time and the flow regime will be site specific [4]. As tides rise and fall they produce flood and ebb currents. A tidal stream turbine (TST) is designed to extract the kinetic energy contained in these currents. The strength of the tidal currents will vary and strong variations in flow speed will exist at any site, with the maximum speeds occurring infrequently [5]. TSTs will be subjected to turbulence and waves, which will cause further variations in flow speed [6]. This means that they need to be regulated, with a way of limiting output power and shedding mechanical load at high flow speeds [7]. Designing a turbine capable of operating at the maximum flow speed seen at a site will not be economic and it will operate at less than 100% capacity for much of the time [8].

Manuscript received April 23, 2013; accepted July 05, 2013. Date of publication August 15, 2013; date of current version December 12, 2013. This work was supported by the Engineering and Physical Sciences Research Council (EPSRC), Research Councils U.K. (RCUK), under Grant “Centre for Integrated Renewable Energy Generation and Supply (CIREGS),” number EP/E036503/1.

The authors are with Cardiff University, Cardiff CF24 3AA, Wales, U.K. (e-mail: WhitbyB@cardiff.ac.uk; Ugalde-LooC@cardiff.ac.uk).

Digital Object Identifier 10.1109/TSTE.2013.2272653

Although developers are still designing different types of TSTs, more than 50% are based on bottom mounted, low solidity, horizontal axial flow rotors [9]. Existing and proposed designs use either variable or fixed pitch blades. Variable pitch turbines vary the pitch angle of the blades to regulate output power. The blades can be pitched to feather as the flow speed increases. This reduces the lift force on the blade; therefore, the torque on the rotor is reduced and power is regulated. Alternatively, the blades can be pitched to actively induce stall above rated flow speed [10]. On the other hand, fixed pitch designs rely on the stall characteristic of the rotor blades to regulate output power. As the TST approaches rated power, the angle of attack is such that the blade begins to stall [11].

A comparison is carried out between a variable-speed pitch regulated turbine where the blades are pitched to feather and a variable-speed stall regulated turbine that has fixed pitch blades. Models of each TST are simulated using the commercially available software GH Tidal Bladed [12]. The dynamic characteristics under both types of regulation are examined and control system design is done in MATLAB. Following control implementation, an analysis in terms of performance under turbulent flows, loading, and energy yield is carried out using Tidal Bladed. The studies show that the dynamics of each turbine model are significantly different for above rated flow speed operation. This has implications on the controller design and the loading experienced by each TST.

II. TIDAL POWER

The power that a TST is able to extract from a tidal flow passing through a perpendicular area is given by [11]

$$P_{hy} = \frac{1}{2} \rho A V_{\text{flow}}^3 C_P(\beta, \lambda) \quad (1)$$

where ρ is the water density, A is the swept area by the rotor, V_{flow} is the flow speed, and C_P is the power coefficient, which describes the efficiency of the TST as a function of the pitch angle of the blades (β) and the tip-speed ratio (λ), defined as

$$\lambda = \frac{\omega_r \cdot R}{V_{\text{flow}}} \quad (2)$$

where ω_r is the rotational speed of the rotor and R the radius.

Although many TSTs have obvious similarities to wind turbines (WTs), several important differences exist. As opposed to WTs, in TSTs the high density of the water leads to large out of plane bending forces on the blades [13]. Moreover, the flow rates are lower for TSTs. WTs are rated for a wind speed in the region of 12–15 m/s [14]. Conversely, the rated flow speed of a TST is between 2–3 m/s [15], [16]. In addition, a TST and a WT of a similar power rating will have a significant difference in rotor size. Consider a 1-MW TST (rated flow speed: 2.4 m/s) and a 1-MW WT (rated wind speed: 15 m/s)

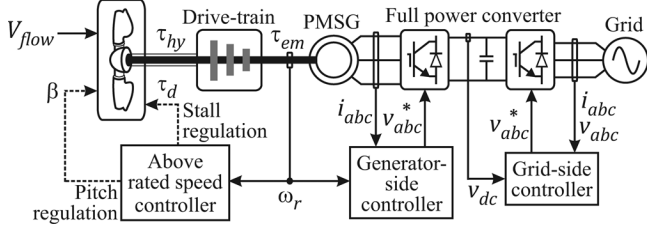


Fig. 1. TST configuration based on a PMSG and an FPC.

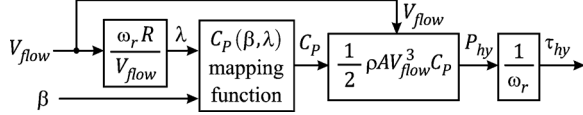


Fig. 2. Model of a hydrodynamic system.

with the same power coefficient. If the water and air densities are 1025 and 1.225 kg/m^3 , respectively, and by using (1), it is clear that the TST is more compact than the WT: the ratio of radii is $R_{TT}/R_{WT} = 0.54$. Furthermore, by assuming that the tip-speed ratio is the same for both turbines and by using (2), the ratio of rotational speeds is $\omega_{r,TT}/\omega_{r,WT} = 0.3$. The fact that TST blades are short and rotate relatively slowly means that centrifugal forces, which balance the bending forces on large WTs, are small. This means they do little to restrict the large bending forces acting on the blades of a TST [17].

III. TST CONFIGURATION AND CONTROL OBJECTIVES

Permanent magnet synchronous generators (PMSGs) are attractive for use in a TST. They do not require an external excitation current; slip rings and brushes are not necessary [18]. In comparison to induction generators, PMSGs operate at a higher power factor and achieve a higher power density [19]. In addition, they may be designed to rotate at very low speeds, eliminating the need for a gearbox. When used in conjunction with a full power converter (FPC), the generator is decoupled from the grid and variable-speed operation can be achieved [14]. Such a configuration is considered in this paper (Fig. 1).

A. Hydrodynamic Model

The hydrodynamic torque developed by the rotor is [20]

$$\tau_{hy} = \frac{1}{2} \cdot \frac{\rho A V_{flow}^3 C_P(\beta, \lambda)}{\omega_r}. \quad (3)$$

The block diagram of a hydrodynamic system is shown in Fig. 2. For modeling purposes, C_P is a mapping function obtained either through a lookup table or an approximating function [21]. The lookup table approach is used in this paper.

B. Drive-Train Model

The hydrodynamic torque is transferred to the generator shaft via the drive-train [22]. A rigid shaft described by

$$\dot{\omega}_r = \frac{1}{J}(\tau_{hy} - \tau_{em}) \quad (4)$$

is assumed in this work, where J is the combined inertia of the rotor, shaft, and generator, and τ_{em} the electromagnetic torque.

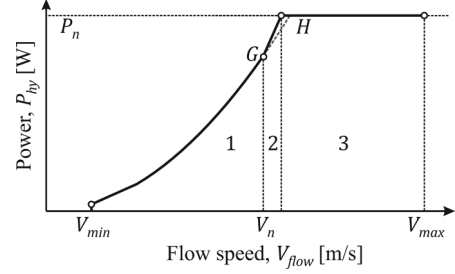


Fig. 3. Power curve of a TST.

C. Structural Dynamics

The TST representation considered in this paper was modeled in Tidal Bladed. Within this software, the blades and the support structure are modeled as single linear flexible components using a modal approach. Only the modal dynamics relating to the blades were considered (four modes in total). Further information is provided in [12].

D. PMSG Model

The generator model is given by [23]

$$\frac{d}{dt} i_d = \frac{1}{L_d} v_d - \frac{R_s}{L_d} i_d + \frac{L_q}{L_d} \omega_r i_q \quad (5)$$

$$\frac{d}{dt} i_q = \frac{1}{L_q} v_q - \frac{L_d}{L_q} \omega_r i_d - \frac{R_s}{L_q} i_q - \frac{1}{L_q} \omega_r \psi_m \quad (6)$$

$$\tau_{em} = \frac{3}{2} n_{PP} [\psi_m + (L_d - L_q) i_d] i_q \quad (7)$$

where L_d, L_q are the self inductances of the stator; R_s the stator resistance; v_d, v_q the stator voltages; i_d, i_q the stator currents; ψ_m the flux linkage of the permanent magnet; τ_{em} the electromagnetic torque; and n_{PP} the number of pole pairs.

E. Generator-Side and Grid-Side Converters [24]

The system (Fig. 1) consists of a PMSG and an FPC with back-to-back VSCs. The generator-side converter controls the operation of the generator. A vector control strategy based on the dynamic model of the PMSG expressed in the dq frame is employed. The grid-side converter transfers the power generated from the turbine to the utility grid and controls the power factor. A vector control scheme is employed, where the dc link voltage (thus, the active power flow into the grid) and the reactive power flow are controlled. Further details on the control and performance are provided in [25].

F. Optimum Flow Power Extraction

The operation and control of WTs for optimal power extraction has been reported comprehensively in the literature [10] and can be equally applied for TSTs. Fig. 3 illustrates the power curve for a typical turbine. As shown, three operating modes are possible. Below the cut-in speed V_{min} the available energy in the flow is so low that turbine operation is uneconomic due to losses and operating costs [14]. In Region 1 (between V_{min} and rated flow speed V_n), the objective is to extract as much energy from the flow as possible by running the turbine at its optimum hydrodynamic efficiency. Region 2 is a transition area between the optimum power curve and the constant power region. Here,

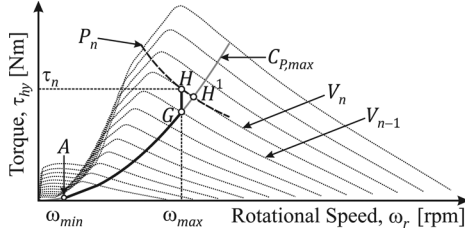


Fig. 4. Variable-speed variable-pitch control strategy (adapted from [10]).

the speed of the turbine is limited to avoid over-speeding the generator and, as a consequence, cavitation [17]. In this region, the turbine moves away from the optimum power curve and operates on GH .

In Region 3 (between H and the cutout speed V_{max}), the objective is to limit power to avoid overloading. Although a substantial energy is available above V_{max} , this occurs so infrequently that operation beyond V_{max} is uneconomic [10].

1) *Power Regulation by Pitching to Feather*: This control strategy is shown in Fig. 4. In low flows, the speed is regulated at ω_{min} . Below rated speed (between A and G), the turbine is operated in variable-speed mode so that the optimum tip-speed ratio is maintained, causing the turbine to follow the $C_{P,max}$ locus. This is achieved by controlling the rotor speed through the generator reaction torque. The generator torque demand τ_d should be set proportional to the square of the measured generator speed [26]

$$\tau_d = \frac{\pi \rho R^5 C_P}{2 \lambda^2 G^3} \cdot \omega_r^2. \quad (8)$$

At G , the rotational speed reaches the upper limit ω_{max} and is, therefore, regulated. The turbine will then operate along segment GH as the flow speed increases from V_{n-1} to V_n . At H , the turbine reaches rated power (along the rated power curve P_n) and the generator torque is held constant at τ_n . In this condition, variations in flow speed reflect in the hydrodynamic torque, resulting in fluctuation of rotational speed and output power. To avoid this and to keep the turbine operating at H the rotor blades must be pitched. This regulates the rotor hydrodynamic torque, thus, regulating the generator speed and producing constant power. In the case where the rotor speed limit is not reached until the flow speed reaches V_n , the torque speed trajectory reduces to AH^1 as opposed to AGH . This is equivalent to removing operating Region 2 in Fig. 3.

2) *Power Regulation by Stall*: Fig. 5 summarizes two schemes for stall regulation: passive (segment $AEDG$) and speed-assisted (segment $ABCDG^1$). Below rated flow speed, both turbines operate in variable-speed mode and track the $C_{P,max}$ locus. The passive stall regulated turbine operates between points A and E . If E is reached, the rotational speed is limited and the turbine follows ED . At D , representing the maximum power that can be generated, the turbine goes into deep stall, with flow separation occurring along the length of the blade. For flow speeds above this point, the hydrodynamic torque reduces and the operation moves back along ED to G . Thus, a passive stall regulated turbine is unable to maintain rated output power. The power falls away as the turbine goes deeper into stall; thus, it is unable to follow the ideal power curve in Fig. 3. Instead, the power curve is shown in Fig. 6.

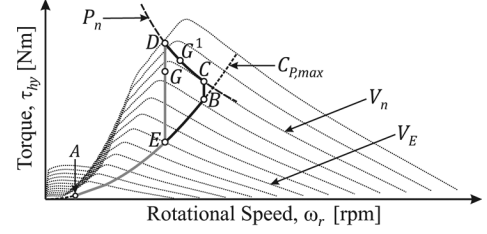


Fig. 5. Variable-speed fixed-pitch control strategies with passive ($AEDG$) and speed-assisted ($ABCDG^1$) stall regulation (adapted from [10]).

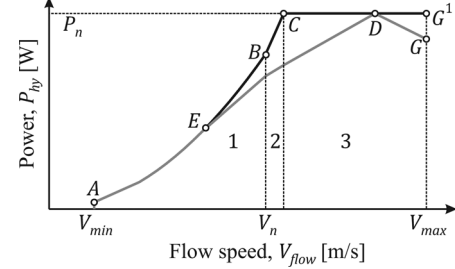


Fig. 6. Power curve for variable-speed fixed pitch control strategies with passive ($AEDG$) and speed-assisted ($ABCDG^1$) stall regulation.

On the other hand, the speed-assisted stall turbine operates between A and B (Fig. 5) for below rated flow speeds. At B , the rotational speed is limited and the turbine follows segment BC , reaching rated power at C . As the flow speed increases, the generator torque is increased to reduce the rotor speed and to drag the rotor into stall, while keeping the turbine operating on the rated power curve P_n . Eventually the turbine goes into deep stall at D and moves back along segment CD to G^1 . The power curve for the assisted stall scheme is shown in Fig. 6—in agreement with that of Fig. 3. For this reason, power regulation by speed-assisted stall is used in this paper.

IV. COMPARISON BETWEEN PITCH & STALL REGULATION

Two generic 1-MW TST models were developed in Tidal Bladed [12]. They were kept as similar as possible to ensure a fair comparison. Their parameters are given in Appendix A.

A. Rotor Design

According to [27], NACA 63 series foils are recommended to define the primary shape of blades for TSTs since they are more resistant to cavitation and less sensitive to leading edge roughness than other foils. An NACA 63–424 airfoil was chosen because it is a relatively thick section (necessary to provide adequate structural strength) while still offering a good lift to drag ratio. The chord distributions for each blade were kept the same in both pitch and stall regulated turbines. Only the twist distributions of each blade [Fig. 7(a)] were varied to obtain the desired operating characteristics.

The twist distribution of the stall regulated blade was chosen such that the rotor blade will operate at a higher angle of attack (closer to stall) and shed power as the flow speed increases [28]. This is confirmed by its narrower C_P curve [Fig. 7(b)]. As discussed in [29], stall regulated turbines commonly have steep peaky C_P curves. In above rated flow speed operation (CD in Fig. 5), the stall regulated TST requires a limited speed reduction to maintain constant power, ensuring that the generator rated torque is kept within limits. Unfortunately, this means that it is less efficient than its pitch counterpart. This is evidenced by

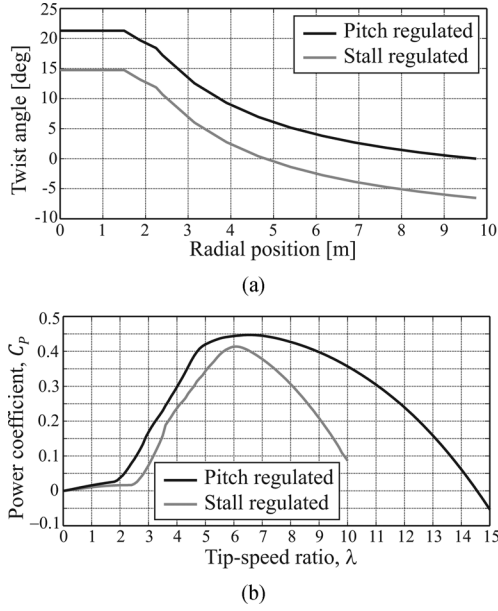


Fig. 7. Design for pitch and stall regulated rotors. (a) Twist angle distribution along blade. (b) C_p curves.

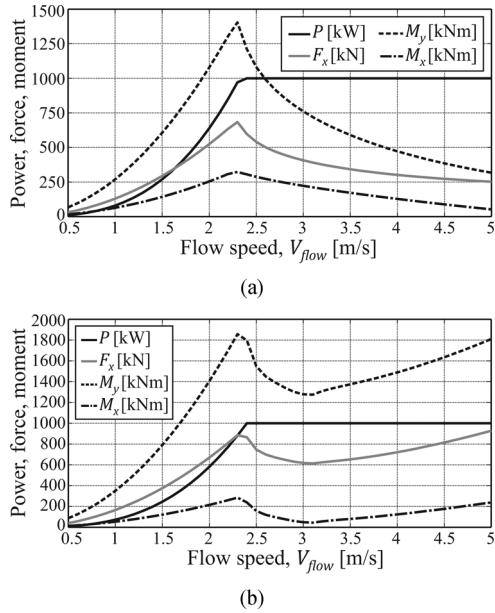


Fig. 8. Steady state outputs as function of flow speed. (a) Pitch regulation. (b) Speed-assisted stall regulation.

the peak C_p values of 0.414 for the stall regulated turbine and 0.447 for the pitch regulated turbine. The result is an increase in axial load for the stall regulated rotor (more force is transferred into axial load rather than into rotating the blade).

Fig. 8 shows the steady state power output, thrust force (F_x), and out-of-plane (M_y) and in-plane blade root bending moments (M_x). M_x acts about an axis parallel to the rotor axis and is mainly driven by inertial and gravitational forces, whereas M_y acts perpendicular to the rotor plane and is primarily driven by F_x [6]. It can be seen that F_x is higher for the stall regulated turbine—due to its twist distribution. M_y dominates in both cases, being higher for the stall regulated TST. In contrast, M_x is significantly lower for both turbines.

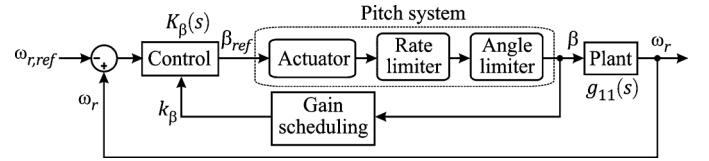


Fig. 9. Pitch angle control for above rated flow speed.

B. Control System Design

In order to compare loads and energy yield under dynamic inflow conditions while considering the modal dynamics of the blades, controllers for both TSTs were designed. The control objectives for either turbine were to optimize the power production for below rated flow speed and to limit the hydrodynamic power above rated flow speed. Below rated, the generator speed was varied by controlling the generator torque to follow an optimal torque versus speed curve. This was derived in Tidal Bladed and specified through a lookup table. Since the electric time constant is much smaller than the mechanical time constant of the system, the electrical dynamics were assumed to be in steady state. Therefore, in this work, the PMSG electrical subsystem and drive were modeled as a first order lag with time constant $\tau = L_q/R_s$.

1) *Pitch Regulated TST Analysis and Control*: Fig. 9 shows the pitch angle control loop for a pitch regulated TST [14]. This is active above rated flow speed, with the torque demand τ_d held constant. It consists of a controller that generates the pitch angle demand β_{ref} from the generator speed error. This is sent to the pitch actuator, with a position limiter ensuring actuator limits are not exceeded.

In order to design the controller, the actuator and plant dynamics were derived using the linearization module of Tidal Bladed. A linearized system of the form

$$\omega_r(s) = g_{11}(s)\beta(s) \quad (9)$$

was then obtained in MATLAB—relating pitch demand β and generator speed ω_r . This was carried out for above rated flow speeds up to 5.0 m/s in steps of 0.1 m/s. The plant was assumed as single-input single-output (SISO), with contributions to the input–output transmittance considered as disturbances. It should be noticed that $g_{11}(s)$ in (9) comprises both the pitch system and plant dynamics transfer functions of the block diagram shown in Fig. 9. The general structure of $g_{11}(s)$ is

$$g_{11}(s) = -k_{11} \cdot \frac{(s + z_{11})}{(s + 5)(s + p_{11})} \cdot \frac{n_{11}(s)}{d_{11}(s)} \quad (10)$$

where k_{11} is a gain, p_{11} is a left-hand plane pole (LHPP) in the range of 2.9–15.4 rad/s; z_{11} is a left-hand plane zero (LHPZ) in the range of 39–79 rad/s; and $n_{11}(s)$ and $d_{11}(s)$ are complex conjugate zeros and poles of high frequency. The frequency in elements of (10) varies with flow speed. Fig. 10(a) shows the Bode plot of all $g_{11}(s)$ as functions of flow speed V_{flow} . Fig. 10(b) shows frequencies before the occurrence of resonances.

Simple inspection of the family of plants (10) shows that they are stable for all flow speeds; however, one nonminimum phase zero pair [or right-hand plane zero (RHPZ)] is present in $n_{11}(s)$. It is well-known that RHPZs impose limitations on the achievable performance [30]. In addition, the presence of weakly damped complex conjugate LHPPs [in $d_{11}(s)$] and LHPZs [in $n_{11}(s)$] results in resonant and inverse resonant

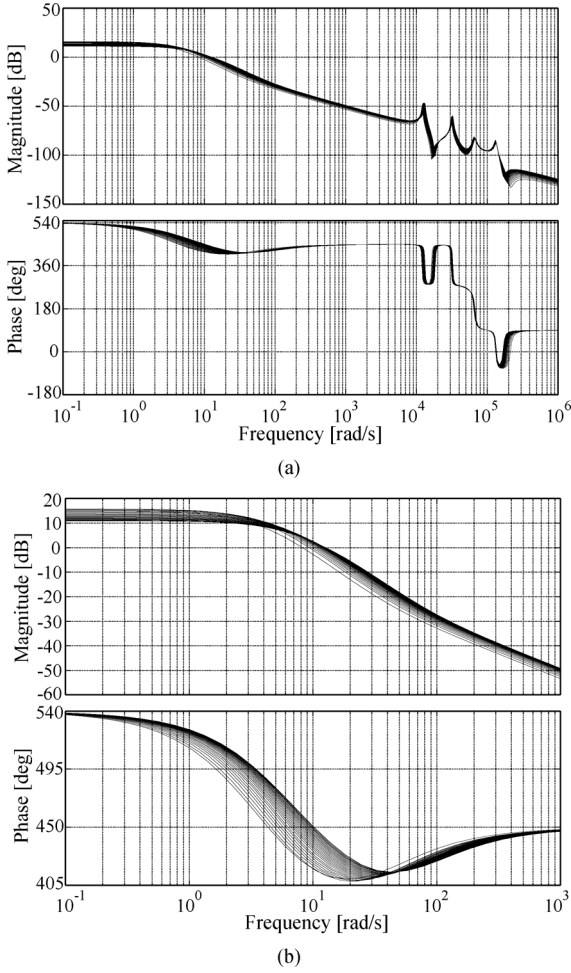


Fig. 10. Bode plots of $g_{11}(s)$. (a) Frequencies including resonant poles and zeros. (b) Low frequencies.

peaks in the magnitude plot and sudden change of phase angle in the phase plot (Fig. 10). To avoid such undesirable dynamics (associated with the blade modes), $K_\beta(s)$ in Fig. 9 should have a restricted bandwidth by at least a decade below 10^4 rad/s.

An appropriate control design for $K_\beta(s)$ is

$$K_\beta(s) = -k_\beta \cdot \frac{(s + 7.5)}{s} \cdot \frac{(s + 12)}{(s + 60)} \quad (11)$$

which was achieved through Bode-shaping. It consists of a PI cascaded with a lead term. Gain k_β in (11) was adjusted to achieve a reasonably similar bandwidth for all plants. The set of gains is given in Appendix B. Fig. 11 depicts the Bode plot of the open loop system $K_\beta(s)g_{11}(s)$ for frequencies below 10^4 rad/s. The bandwidth is in the region of 300–490 rad/s. The control design has good stability margins for all cases (phase margin: $M_{ph} > 85^\circ$; gain margin: $M_g \approx 10$ dB) through the inclusion of the additional lead term. These characteristics reflect in an adequate step response, shown in Fig. 12.

2) *Stall Regulated TST Analysis and Control*: A number of methods for controlling speed-assisted stall regulated TSTs are discussed in [29], [31], and [32]. In [29], a Kalman filter is proposed to estimate the hydrodynamic torque by using a measurement of the generator rotational speed. The speed reference would be

$$\omega_{r,ref} = \frac{P_{max}}{\hat{\tau}_{hy}} \quad (12)$$

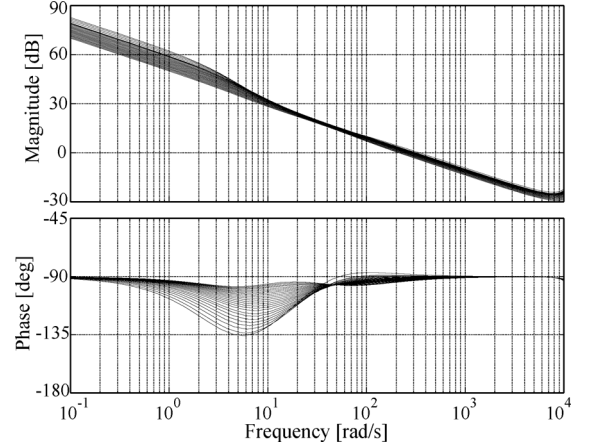


Fig. 11. Performance assessment of the pitch control loop. Bode plots of $K_\beta(s)g_{11}(s)$ for frequencies below 10^4 rad/s.

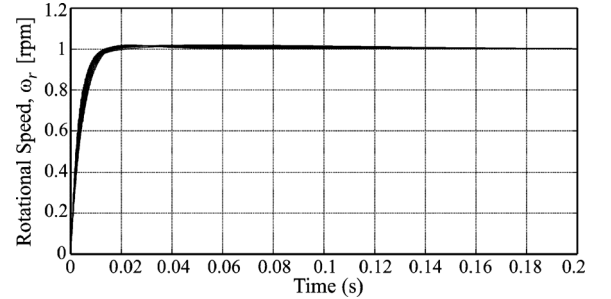


Fig. 12. Performance assessment of the pitch control loop: step responses.

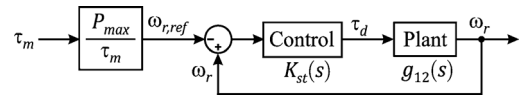


Fig. 13. Variable-speed stall regulated control strategy.

where P_{max} is the rated power and $\hat{\tau}_{hy}$ is the estimated hydrodynamic torque. In this work, speed regulation was achieved under the assumption that the turbine's low speed shaft torque τ_m is available, with the speed reference being calculated with (12). This is shown in Fig. 13. In reality, there may be practical difficulties achieving a torque measurement, which could be avoided through the use of an observer-based controller as in [29]. However the use, design, and implementation of observers are out of the scope of this paper.

Following a similar procedure as for the pitch regulated turbine, a family of SISO plants relating generator torque demand τ_d and generator speed ω_r was obtained

$$\omega_r(s) = g_{12}(s)\tau_d(s) \quad (13)$$

with structure

$$g_{12}(s) = \frac{-k_{12}}{(s + 10)(s - p_{12})} \cdot \frac{n_{12}(s)}{d_{12}(s)} \quad (14)$$

where k_{12} is a gain, p_{12} is an RHPP in the range of 0.4–17.7 rad/s, and $n_{12}(s)$ and $d_{12}(s)$ are complex conjugate zeros and poles of high frequency. The frequencies of elements in (14) vary with flow speed. Fig. 14(a) illustrates the Bode plot of $g_{12}(s)$ as a function of flow speed V_{flow} . Fig. 14(b) shows the Bode plots before the occurrence of the resonances.

It is clear from (14) that $g_{12}(s)$ are unstable due to the presence of p_{12} —the low frequency RHPP, which is caused by the

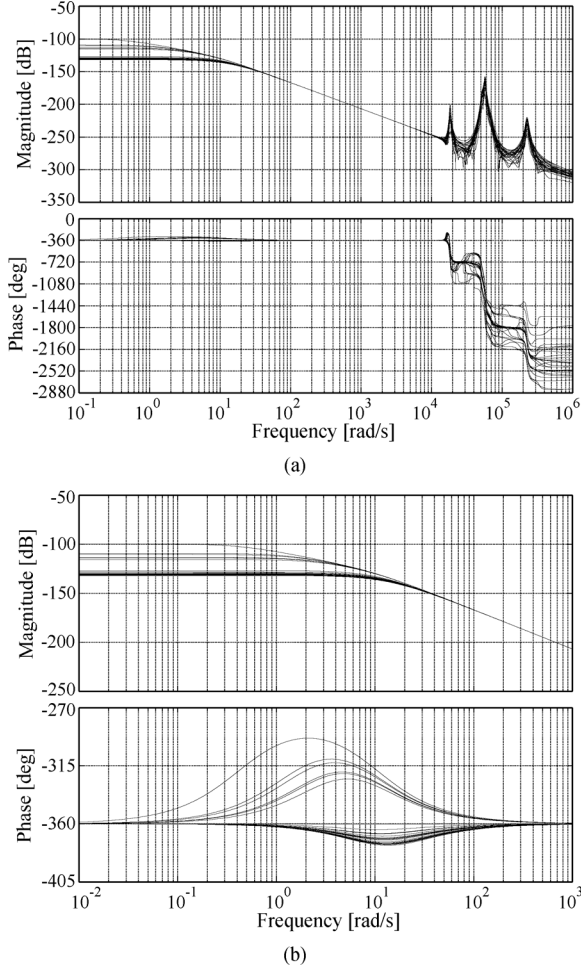


Fig. 14. Bode plots of $g_{12}(s)$. (a) Frequencies including resonant poles and zeros. (b) Low frequencies.

hydrodynamics and varies with the operating point. Such instability is not unique to the model in this paper but is always the case [33]. Moreover, at least five complex pairs of RHPZs appear in each $n_{12}(s)$. As opposed to the pitch regulated TST, the controller should not only restrict the bandwidth below the frequencies of the RHPZs, but also stabilize the plant. The complex RHPZs and LHPZs of $n_{12}(s)$ and LHPPs of $d_{12}(s)$ occur at high frequencies and are weakly damped. These characteristics are reflected in resonant and inverted resonant peaks in the magnitude plot and sudden change of phase in the phase plot (Fig. 14). Losses in phase are greater than in pitch regulation due to the additional RHPZs.

It is important to highlight that above $V_{\text{How}} = 3.1$ m/s the frequency of RHPP p_{12} is greater than that of the LHPP pole (10 rad/s). This occurs when the TST is entering into deep stall. Based on the previous analysis, two controllers were designed: one for operation above rated flow speeds up to 3.0 m/s and an additional for above 3.0 m/s. The bandwidth was restricted by at least a decade below 10^4 rad/s. Appropriate designs, achieved through Bode-shaping are

$$K_{st1}(s) = -k_{s1} \cdot \frac{(s + 0.25)}{s} \cdot \frac{(s + 7)}{(s + 60)} \quad (15)$$

$$K_{st2}(s) = -k_{s2} \cdot \frac{(s + 4.25)}{s} \cdot \frac{(s + 4.5)}{(s + 120)} \quad (16)$$

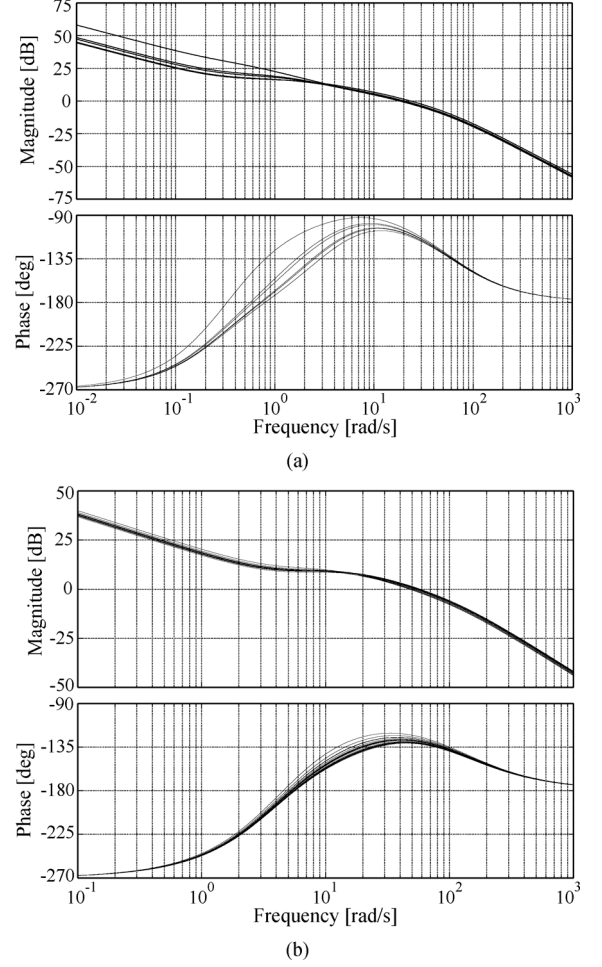


Fig. 15. Performance assessment of the speed-assisted stall control loop: Bode plots for frequencies below 10^3 rad/s. (a) Before deep stall. (b) After deep stall.

with (15) being active above rated flow speeds up to 3.0 m/s, switching to (16) for higher speeds. The structure of (15) and (16) consists of a PI cascaded with a lead term that improves stability margins. Gains k_{s1} and k_{s2} were adjusted to achieve a similar bandwidth for the flow speeds in which (15) and (16) are active. These gains are given in Appendix B.

The Bode plots of $K_{st1}(s)g_{12}(s)$ and $K_{st2}(s)g_{12}(s)$ are shown in Fig. 15. The bandwidth before deep stall is in the region of 20–32 rad/s and 64–78 rad/s after the TST enters into deep stall. The control design features good stability margins (before deep stall: $M_{ph} > 65^\circ$; $M_g \approx 100$ dB; after deep stall: $M_{ph} > 45^\circ$; $M_g \approx 80$ dB).

The step response of the control system is shown in Fig. 16. The performance worsens when the turbine enters into deep stall, as shown in Fig. 16(b). An improved performance could be achieved by using a more complex controller; however, the simplicity and insight offered by (15) and (16) would be lost.

C. Performance and Loading Analysis

To test the performance of the controllers from Section IV-B, hydroelastic simulations were run in Tidal Bladed under time varying environmental conditions. They were carried out following a digital implementation in C++ code, compiled as a dynamic link library (DLL) as discussed in [12]. To this end, the discrete versions of (11), (15), and (16) were obtained using

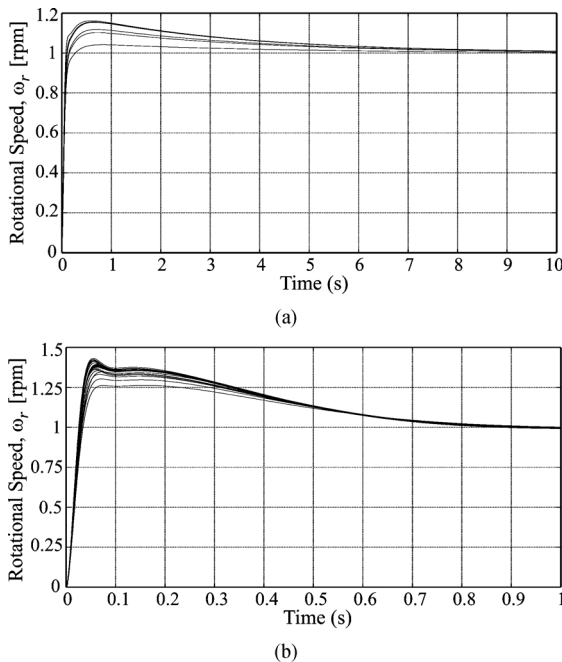


Fig. 16. Performance assessment of the stall control loop: step responses. (a) Before deep stall. (b) After deep stall.

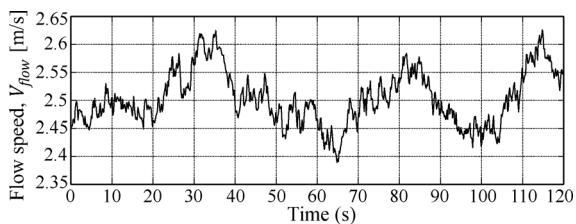


Fig. 17. Hub height flow speed with longitudinal turbulence intensity of 5%.

the zero-order-hold method with a sampling time of 1 kHz [34], [35]. A discrete time-step of 0.001 s was used.

The hub height flow speed used (Fig. 17) was generated by defining a mean speed of 2.6 m/s and imposing a turbulence intensity of 5% using the von Karman spectral model. Tower shadow effects and structural dynamics of the blades were included [12]; those of the support structure were not.

Fig. 18(a) shows the rotational speeds for the variable-speed pitch and speed-assisted stall regulated TSTs. As expected, the rotor speed of the pitch regulated machine is regulated at rated speed (13 rpm) and as a result the output power, shown in Fig. 18(b), is also regulated at the rated value of 1000 kW. For the stall regulated TST, the rotor speed varies as the reference generated by (12) is tracked. The resulting power is shown in Fig. 18(b). The power regulation of the pitch regulated TST is superior to that of the stall regulated machine.

The thrust force (F_x) and out-of-plane (M_y) and in-plane blade root bending moments (M_x) are shown in Fig. 19(a)–(c). It can be seen that F_x is higher for the stall regulated turbine [Fig. 19(a)]. This is due to the twist distribution of the stall regulated blade. M_y dominates in both cases, being higher for the stall regulated TST [Fig. 19(b)]. In contrast, M_x is significantly lower for both turbines [Fig. 19(c)]. These results confirm that the out-of-plane bending forces are dominant and higher for the speed-assisted stall regulated TST.

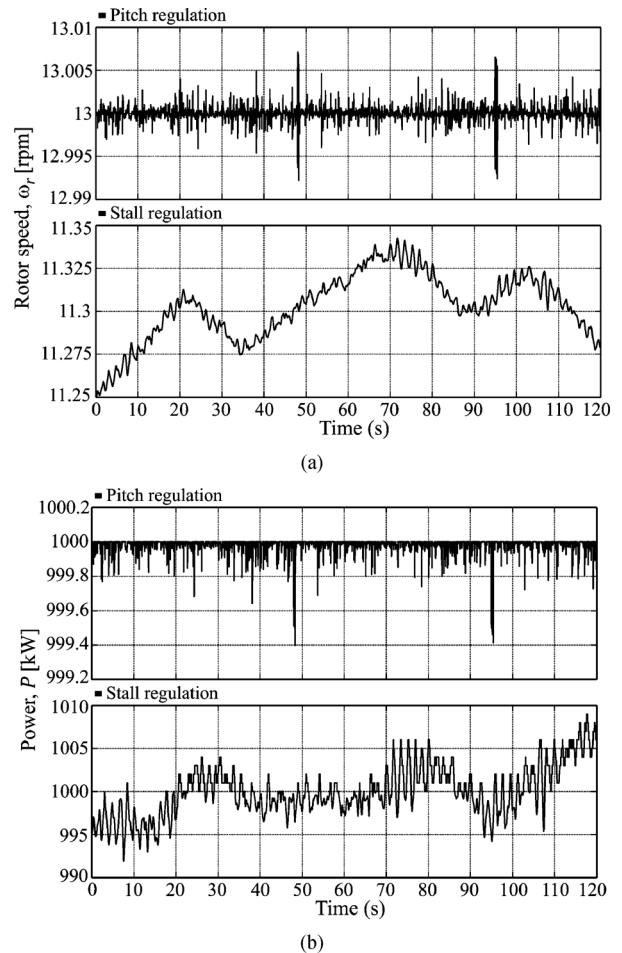


Fig. 18. Rotor speed and output power for pitch and stall regulated TSTs. (a) Rotor speed (ω_r). (b) Output power (P).

D. Annual Energy Yield Analysis

The dynamic power curves shown in Fig. 20 were used to calculate the energy yield for each turbine. This includes the effect of the controller performance. A 100% availability of the TSTs was assumed. Calculations were carried out in Tidal Bladed, resulting in 5.436 GWh p.a. for the pitch regulated turbine and 5.299 GWh p.a. for the speed-assisted stall regulated turbine. The superior performance of the pitch regulated TST is mainly due to the better performance of the pitch controller and a more efficient blade design—it operates at a higher C_P value below rated flow speed.

V. CONCLUSION

A performance comparison and control system design was carried out for pitch and stall regulated horizontal axial flow, variable-speed TSTs. Following system linearization in Tidal Bladed, an analysis of the model dynamics was undertaken in MATLAB. Below rated flow speed, the dynamics of both TST models are stable. However, above rated flow speed the dynamics are significantly different: the pitch regulated TST is stable, whilst the stall regulated TST has unstable dynamics. Both turbines feature RHPZs. Therefore, controlling the stall regulated TST is more onerous as the controller has to stabilize the plant while restricting the bandwidth below the frequencies of the RHPZs.

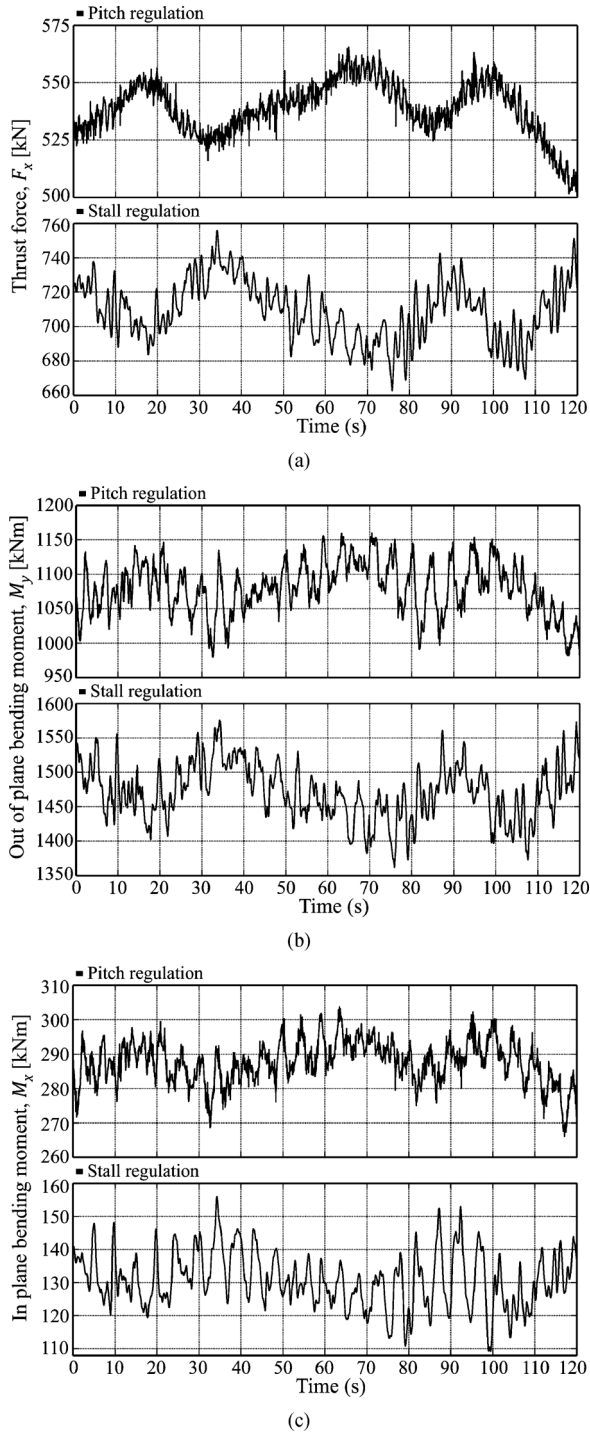


Fig. 19. Thrust and bending moments for pitch and stall regulated TSTs. (a) Rotor thrust force (F_x). (b) Out-of-plane blade root bending moment (M_y). (c) In-plane blade root bending moment (M_x).

Controllers were designed in MATLAB for both TST models, providing a satisfactory performance when implemented and tested in Tidal Bladed. Although the controller structure was kept as simple as possible to make implementation easier, the designs ensured adequate stability margins. It is clear from the results that the power regulation of the pitch regulated TST was superior.

Analyses of the loads showed that the out-of-plane bending moments dominate and are higher for the stall regulated TST

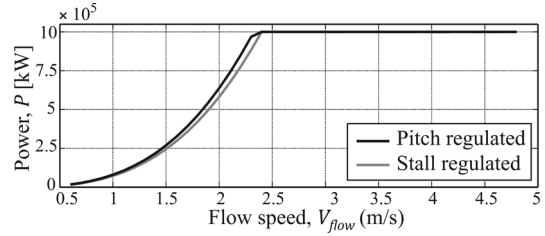


Fig. 20. Dynamic power curves.

over the entire operating range of the turbine. In fact, they are significantly higher when the turbine goes into deep stall. This is because the axial thrust force is higher, which results from the fact that the blades were designed to operate at a higher angle of attack, near to the maximum lift coefficient.

Regarding the energy yields, the one obtained for the pitch regulated TST was higher. This is largely because the pitch regulated turbine is more efficient below rated flow speed; in addition, the superior performance of the pitch controller also has an effect. It should be noted that 100% availability of the turbines was assumed when carrying out this calculation. In reality, this will not be the case and one could argue that the increased complexity of the pitch machine (which requires pitch bearings, hydraulic actuators and position sensors) will mean more maintenance and increased downtime.

Designers looking to choose between the pitch and speed-assisted stall regulation methods will need to be aware of the higher out-of-plane loads generated by the stall regulated TST—especially in high flow speeds, as the axial thrust force will increase unchecked as the flow speed increases. This, together with the increased complexity of the controller would suggest that the fixed pitch speed-assisted stall regulated turbine will need to be much cheaper in order to compete with variable pitch regulated turbines on a lifetime cost basis. However, this conclusion assumes that the availability of both TSTs is comparable—something requiring further investigation.

APPENDIX

A. Tidal Stream Turbine Parameters

TSTs: Power rating = 1 MW; Rated speed ω_r = 13 rpm; Rated hub flow speed V_{flow} = 2.4 m/s; Rotor diameter R = 21.3 m; Blade length = 9.75 m; Water depth = 50 m; Hub height above sea-bed = 29 m; Rotor blades = 3; Rotor position = upstream. *Tip-speed ratio below rated flow speed*: Assisted-stall regulated TST, λ = 5.9. Pitch regulated TST, λ = 6.4.

Generator: Output power: 1 MW, Pole pairs = 60; Freq. = 50 Hz; R_s = 4.61 m Ω ; L_d = L_q = 886.48 μ H; ψ_m = 6.8973 Vs.

B. Pitch and Stall Controller Gains Above Rated Flow Speed

Flow speeds from 2.5–5 m/s. Gains given for steps of 0.1 m/s.

Pitch:

$$k_{\beta} = [162.5, 135, 125, 115, 107.5, 107.5, 107.5, 105, 102.5, 100, 97.5, 95, 92.5, 90, 87.5, 85, 82.5, 80, 77.5, 75, 72.5, 70, 67.5, 65, 62.5, 60].$$

Stall (from 2.5–3 m/s):

$$k_{s1} = 10^6 \cdot [26.68, 26.68, 29, 26.68, 34.8, 30.16]$$

Stall (from 3.1–5 m/s):

$$k_{s2} = 10^6 \cdot [139.2, 145, 174, 145, 156.6, 150.8, 168.2, 168.2, 165.88, 174, 162.4, 171.68, 162.4, 174, 179.8, 179.8, 179.8, 179.8, 179.8].$$

ACKNOWLEDGMENT

The authors thank Prof. N. Jenkins and Dr. J. Liang for their contributions to this work. The authors also thank GL Garrad Hassan for the use of Tidal Bladed and their support.

REFERENCES

- [1] Black and Veatch, UK Tidal Current Resource and Economics Study Report, The Carbon Trust, 2011.
- [2] Quantification of Exploitable Tidal Energy Resources in UK Waters, ABP Marine Environmental Research Ltd., 2007.
- [3] Accelerating Marine Energy, Carbon Trust, 2011.
- [4] G. McCann, M. Thomson, and S. Hitchcock, "Implications of site-specific conditions on the prediction of loading and power performance of a tidal stream device," in *Proc. 2nd Int. Conf. Ocean Energy (ICOE)*, Brest, France, 2008.
- [5] I. G. Bryden, "Tidal energy," in *Encyclopedia of Energy*. New York, NY, USA: Elsevier, 2004, pp. 139–150.
- [6] I. A. Milne, R. N. Sharma, R. G. J. Flay, and S. Bickerton, "The role of onset turbulence on tidal turbine blade loads," in *Proc. 17th Australasian Fluid Mechanics Conf.*, Auckland, New Zealand, 2010.
- [7] P. Fraenkel, "Practical tidal turbine design considerations," in *Proc. Ocean Power Fluid Machinery Seminar*, London, U.K., 2010, pp. 1–19.
- [8] J. King and T. Tryfonas, "Tidal stream power technology—State of the art," in *Proc. OCEANS-EUROPE*, 2009, pp. 1–8.
- [9] Training Course Manual: Introduction to Wave and Tidal Energy Conversion, Garrad Hassan & Partners Ltd., Bristol, U.K., 2010.
- [10] F. Bianchi, H. de Battista, and R. J. Mantz, *Wind Turbine Control Systems: Principles, Modelling and Gain Scheduling Design*. New York, NY, USA: Springer, 2007.
- [11] J. F. Manwell, J. G. McGowan, and A. L. Rogers, *Wind Energy Explained: Theory, Design and Application*. Hoboken, NJ, USA: Wiley, 2009.
- [12] E. A. Bossanyi, GH Tidal Bladed Theory Manual, Garrad Hassan & Partners Ltd., 2009.
- [13] G. Marsh, "Tidal turbines harness the power of the sea," *Reinforced Plastics*, vol. 48, no. 6, pp. 44–47, 2004.
- [14] T. Burton, D. Sharpe, N. Jenkins, and E. A. Bossanyi, *Wind Energy Handbook*. Hoboken, NJ, USA: Wiley, 2002.
- [15] P. Bornens, J. Daviau, L. Gaillard, A. Guerrier, and J. Ruer, "The Sabella Tidal Turbine—Test Results and further development," in *Proc. 3rd Int. Conf. Ocean Energy (ICOE)*, Bilbao, Spain, 2010.
- [16] P. Fraenkel, "Development and testing of Marine Current Turbine's SeaGen 1.2 MW tidal stream turbine," in *Proc. 3rd Int. Conf. Ocean Energy (ICOE)*, Bilbao, Spain, 2010.
- [17] P. L. Fraenkel, "Power from marine currents," *Proc. Inst. Mech. Eng., Part A: J. of Power and Energy*, vol. 216, no. 1, pp. 1–14, 2002.
- [18] P. Pillay and R. Krishnan, "Modeling, simulation, and analysis of permanent-magnet motor drives. I. The permanent-magnet synchronous motor drive," *IEEE Trans. Ind. Appl.*, vol. 25, no. 2, pp. 265–273, Mar./Apr. 1989.
- [19] M. J. Melfi, S. Evon, and R. McElveen, "Induction versus permanent magnet motors," *IEEE Ind. Appl. Mag.*, vol. 15, no. 6, pp. 28–35, Nov./Dec. 2009.

- [20] D. Bourlis, "A complete control scheme for variable speed stall regulated wind turbines," in *Fundamental and Advanced Topics in Wind Power*, R. Carriveau, Ed. Vienna, Austria: InTech, 2011, ch. 14, pp. 309–339 [Online]. Available: <http://www.intechopen.com/books/fundamental-and-advanced-topics-in-wind-power/a-complete-control-scheme-for-variable-speed-stall-regulated-wind-turbines>
- [21] S. Heier, *Grid Integration of Wind Energy Conversion Systems*, 2nd ed. Hoboken, NJ, USA: Wiley, 2006.
- [22] J. Licari, C. E. Ugalde-Loo, J. Liang, J. Ekanayake, and N. Jenkins, "Torsional damping considering both shaft and blade flexibilities," *Wind Eng.*, vol. 36, no. 2, pp. 181–196, 2012.
- [23] R. Krishnan, *Permanent Magnet Synchronous and Brushless DC Motor Drives*. New York, NY, USA: Taylor & Francis, 2010.
- [24] R. Peña, J. C. Clare, and G. M. Asher, "Doubly fed induction generator using back-to-back PWM converters and its application to variable speed wind-energy generation," *Proc. Inst. Elect. Eng. Elect. Power Appl.*, vol. 143, no. 3, pp. 231–241, 1996.
- [25] J. Liang and B. Whitby, "Field oriented control of a permanent magnet synchronous generator for use in a variable speed tidal stream turbine," in *Proc. 46th Int. Univ. Power Eng. Conf. (UPEC)*, Soest, Germany, 2011, pp. 1–6.
- [26] E. A. Bossanyi, "Wind turbine control for load reduction," *Wind Energy*, vol. 6, no. 3, pp. 229–244, 2003.
- [27] G. S. Bir, M. J. Lawson, and Y. Li, "Structural design of a horizontal-axis tidal current turbine composite blade," in *Proc. ASME 30th Int. Conf. Ocean, Offshore, Arctic Eng.*, Netherlands, 2011.
- [28] A. S. Mercer and E. A. Bossanyi, "Stall regulation of variable speed HAWTS," in *Proc. Eur. Wind Energy Conf. (EWEC)*, Gothenburg, Sweden, 1996, vol. 96, pp. 825–828.
- [29] D. Bourlis and J. A. M. Bleijs, "Control of stall regulated variable speed wind turbine based on wind speed estimation using an adaptive Kalman filter," in *Proc. Eur. Wind Energy Conf. (EWEC)*, Warsaw, Poland, 2010, vol. 6, pp. 4699–4710.
- [30] J. S. Freudenberg and D. Looze, "Right half plane poles and zeros and design tradeoffs in feedback systems," *IEEE Trans. Autom. Control*, vol. 30, no. 6, pp. 555–565, Jun. 1985.
- [31] T. Ekelund, "Speed control of wind turbines in the stall region," in *Proc. IEEE Conf. Control Appl. (CCA)*, Glasgow, U.K., 1994, pp. 227–232.
- [32] B. Boukhezzer and H. Siguerdidjane, "Nonlinear control of variable speed wind turbines for power regulation," in *Proc. IEEE Conf. Control Appl. (CCA)*, Toronto, Canada, 2005, vol. 6, pp. 114–119.
- [33] W. E. Leithead and B. Connor, "Control of variable speed wind turbines: Dynamic models," *Int. J. Control*, vol. 73, pp. 1173–1188, 2000.
- [34] R. C. Dorf and R. H. Bishop, *Modern Control Systems*, 11th ed. Upper Saddle River, NJ, USA: Pearson Education Inc., 2007.
- [35] Simulink®7 User's Guide, The MathWorks Inc., 2010.



Ben Whitby (SM'12) was born in Harare, Zimbabwe, in 1984. He graduated from the University of Exeter, U.K., in July 2007, with the M.Eng. (Hons.) degree in electronic engineering. He spent three years working in the renewable energy and power electronics sectors before joining the Institute of Energy within Cardiff University, Wales, U.K., as a Ph.D. student in 2010.

His research is focused on control and design of axial flow tidal stream turbines.



Carlos E. Ugalde-Loo (M'02) was born in Ciudad de México, México, in 1980. He received the B.Sc. degree in electronics and communications engineering from ITESM, México, the M.Sc. degree in electrical engineering from IPN, México, and the Ph.D. degree in electronics and electrical engineering from the University of Glasgow, Scotland, U.K., in 2002, 2005, and 2009, respectively.

In 2010, he joined the Institute of Energy within Cardiff University, Wales, U.K., and is currently Lecturer in Electrical Power Systems. His research inter-

ests include power systems, renewable energy generation, and control.